

## Effects of Iron on Efficacy of Photodynamic Therapy Using Photolon in a Mouse Model of CT26 Colon Cancer

Jung In Lee<sup>1</sup>, Tae-Gyu Ahn<sup>2</sup> and Ji Hyun Choi<sup>2</sup>

<sup>1</sup>Department of Internal Medicine, Chosun University College of Medicine, Gwangju, Korea

<sup>2</sup>Department of Obstetrics and Gynecology, Chosun University College of Medicine, Gwangju, Korea

**Background:** Photodynamic therapy (PDT)-a minimally invasive anti-cancer therapy-is undergoing experimental studies to increase its anti-cancer effects. This study investigated the influence of iron on the anti-cancer effects of PDT.

**Methods:** PDT was performed in a cancer-bearing mouse model, which was created by using a murine colon carcinoma (CT26) cell line after administration of Photolon and iron. Tumor volume and the results of TdT-mediated dUTP-biotin nick end labeling (TUNEL), 8-OHdG, and TBARS assays were used to measure anti-cancer effect.

**Results:** On day 14, tumor volume had increased by 49% in the PDT group and decreased by 72% in the iron+PDT group. The percentage of TUNEL-positive cells in tumor tissues was 45% in the PDT group and 69% in the iron+PDT group, suggesting that the proportion of TUNEL-positive cells had increased in the iron+PDT group. The 8-OHdG content in tumor tissues was 33% higher in the iron+PDT group than in the PDT group. The TBARS content in tumor tissues was 46% higher in the iron+PDT group than in the PDT group.

**Conclusions:** Iron enhances the anti-cancer effect of PDT using Photolon, most likely by increasing oxidative damage. (J Nippon Med Sch 2023; 90: 41-49)

**Key words:** photodynamic therapy, iron, anti-cancer

### Introduction

Cancer is a continuing threat to human health. Basic cancer treatments include surgery, radiation therapy, chemotherapy, and immunotherapy. However, the survival rate of patients with cancer has not increased significantly<sup>1</sup>. Therefore, to enhance the efficacy of cancer treatment, researchers are exploring combination therapies, in which various other treatment methods are performed in parallel with existing treatment methods, and development of new treatments and methods<sup>2</sup>.

Photodynamic therapy (PDT) is a method of cancer treatment that uses a photosensitizer and light. PDT has received attention as an alternative cancer treatment because it has very few side effects and is a minimally invasive therapy that imposes much less treatment burden than chemotherapy and radiation therapy<sup>3</sup>. However, be-

cause of lack of confidence in its effectiveness, PDT has not been widely used as an anti-cancer treatment. Therefore, research is underway to enhance the effectiveness of PDT in combination with chemotherapy, immunotherapy, radiation therapy, and other therapies<sup>4</sup>.

The photosensitizer used in PDT is activated by irradiation with light of a specific wavelength. The activated photosensitizer acts on oxygen molecules to generate reactive oxygen species (ROS) that damage cancer cells, resulting in therapeutic effects<sup>5</sup>. ROS are normally produced in cell mitochondria; however, production of ROS is increased by UV radiation, heavy metals, and drugs, which can cause cell damage<sup>6</sup>. Metal ions are important in various cellular functions. Redox-active metals such as iron, copper, and chromium can continuously produce ROS through the oxidation-reduction cycle<sup>7</sup>. Iron-induced

Correspondence to Ji Hyun Choi, Department of Obstetrics and Gynecology, Chosun University College of Medicine, 309 Pilmun-daero, Dong-gu, Gwangju 61452, Korea

E-mail: choijh@chosun.ac.kr

[https://doi.org/10.1272/jnms.JNMS.2023\\_90-108](https://doi.org/10.1272/jnms.JNMS.2023_90-108)

Journal Website (<https://www.nms.ac.jp/sh/jnms/>)

cytotoxicity can cause a unique type of cell death, ferroptosis, which is completely different from necrosis or apoptosis<sup>8</sup> and is a known strategy for killing cancer cells<sup>9</sup>. Therefore, agents that induce ferroptosis have been suggested as anti-cancer drugs<sup>10</sup>. Erastin induced ferroptosis in oral tongue squamous cell carcinoma and enhances the therapeutic effect of PDT using chlorin e6<sup>11</sup>. It induces ferroptosis by inhibiting the cystine-glutamate antiporter (system xc-)<sup>12</sup>.

Iron chelators that inhibit ferroptosis enhance the efficacy of PDT by photosensitizers derived from 5-aminolaevulinic acid or protoporphyrin IX<sup>13,14</sup>. Iron chelators such as CP94 and AP2-18 increase the amount of protoporphyrin IX in cancer cells<sup>15,16</sup>. Therefore, administration of an iron chelator and a photosensitizer derived from 5-aminolaevulinic acid or protoporphyrin IX increases the amount of photosensitizer in cells, thereby increasing the therapeutic effect of PDT<sup>14,15</sup>.

Zhu et al.<sup>11</sup> reported that ferroptosis enhanced the efficacy of PDT. However, few studies have examined the effect of iron administration on inducing ferroptosis in cancer cells during PDT. This study assessed the therapeutic efficacy of PDT with iron administration using chlorin e6 in a mouse model of colon cancer.

## Materials and Methods

### Materials

Venoferrum, an iron preparation for injections, was purchased from JW Pharmaceutical (Seoul, Korea). Fetal bovine serum (FBS), streptomycin, penicillin, and Dulbecco's modified Eagle's medium (DMEM) were purchased from Gibco BRL (Rockville, MD, USA). Photolon was donated by the Research Department at Dongsung Bio Pharm (Seoul, Korea).

### Cell Culture and in Vitro PDT

The mouse colon cancer cell line CT26 was purchased from the American Type Culture Collection (Manassas, VA, USA). CT26 cells were cultured in DMEM with 10% (v/v) FBS, 10 units/mL penicillin, and 10 µg/mL streptomycin and incubated in an atmosphere of 5% CO<sub>2</sub> at 37°C.

CT26 cells (1 × 10<sup>4</sup> cells per well) were seeded into 96-well plates and incubated overnight at 37°C. After that, CT26 cells were treated with various concentrations of Photolon (0, 1, 2, 4, 6, 8, 10, and 12 µg/mL) and Venoferrum (0, 4, 8, and 12 µg of iron/mL) for 3 h. Next, the media was removed and the cells were washed with Phosphate Buffer Saline (PBS), after which phenol red-free DMEM containing 10% FBS was added. The cells were

irradiated with a light dose of 3 J/cm<sup>2</sup> by using a semiconductor laser device (UPL PDT laser; BelOMO, Minsk, Belarus, λ=660 ± 5 nm). Cellular viability was measured at 24 h after irradiation of the cells by using an MTT (3-(4,5-dimethyl-2-thiazolyl)-2,5-diphenyl-2H-tetrazolium bromide) assay kit (Abcam Cambridge, UK) according to the manufacturer's instructions. The optical density value of each well was measured at 570 nm with a microplate reader (BioTek, Winooski, VT, USA).

### Lipid Peroxidation Assay

Levels of lipid peroxidation products were measured using a thiobarbituric acid reactive substances (TBARS) method. The cells were seeded in 3-cm Petri dishes (Nunc) at a density of 2 × 10<sup>5</sup> cells/dish and incubated for 24 h. After that, CT26 cells were treated with Photolon (6 µg/mL) and Venoferrum (4 and 8 µg of iron/mL) for 3 h. After 3 h, the cells were washed with PBS, after which DMEM (without phenol red and FBS) was added. The cells were irradiated with a light dose of 3 J/cm<sup>2</sup> at a wavelength of 660 nm with a semiconductor laser device and incubated for 4 h. After 4 hours, cells were collected by treatment with 0.05% Trypsin-EDTA solution (Sigma), and levels of TBARS in cells were measured with an OxiSelect TBARS Assay Kit (Cell Biolabs, San Diego, CA, USA) according to the manufacturer's instructions. Briefly, the sample was mixed with 100 µL of SDS lysis solution, reacted with 250 µL of TBA reagent, and centrifuged to collect the supernatant, which was used as n-butanol extraction samples. The butanol extraction sample was extracted by using the same volume of butanol, which was used to quantify TBARS by measuring absorbance at 532 nm.

### Establishing the Colon Cancer-Bearing Mouse Model

Male Balb/c mice (age 6 weeks) were purchased from Samtako Bio Korea (Seoul, Korea) and housed in an environment with a 12-h dark/light cycle, a temperature of 20 ± 2°C, and relative humidity of 60 ± 5%. All animal experiments were conducted in accordance with the relevant ethical regulations and the approval of the Animal Use and Care Committee of Chosun University (approval number: CIACUC 2020-A0040).

CT26 cells (1 × 10<sup>5</sup> cells/mouse) were injected subcutaneously into the dorsal side of the mouse. After injection, the mice were observed over time, and tumor size was measured with a digital caliper. Tumor volume was calculated by using the equation tumor volume (mm<sup>3</sup>) = (width<sup>2</sup> × length)/2.

### In Vivo PDT

Among the experimental animals, mice with a tumor

volume of 350 mm<sup>3</sup> or larger were randomly divided into 4 groups (n = 8 mice/group) as follows: control, iron, PDT, and iron+PDT groups.

Photolon (10 mg) was dissolved in 100 mL of physiological saline and injected into the peritoneal cavity of the mice at a dose of 5 mg/kg body weight. Venoferrum was diluted to a concentration of 10 mg/100 mL of iron in physiological saline and injected intraperitoneally into the mice 2 h after the Photolon injection at a dose of 5 mg/kg of the mouse's body weight. Three hours after intraperitoneal injection of Photolon, the surface of the carcinoma was irradiated with a semiconductor laser device (UPL PDT laser; BelOMO, Minsk, Belarus,  $\lambda=660 \pm 5$  nm).

Twenty-four hours after laser irradiation, 3 animals in each experimental group were sacrificed by cervical dislocation and the tumor masses were excised. Half the tumor masses were used as samples to measure the amount of 8-hydroxy-2-deoxyguanosine (8-OHG) and TBARS. The remaining tumor masses were used as samples for hematoxylin and eosin (H&E) staining and TdT-mediated dUTP-biotin nick end labeling (TUNEL) staining after fixation in 4% paraformaldehyde. In 5 mice in each experimental group, the size of the tumor mass was measured up to 14 days before and after laser irradiation, and photographs were taken.

#### TUNEL Assay

Tissues fixed in 4% paraformaldehyde were embedded in paraffin, and sections were cut to a thickness of 4  $\mu$ m. Paraffin was removed by placing the sections in xylene (twice for 15 min) and ethanol (100%, 95%, 85%, 70%, and 50% each for 5 min). Tissue sections were stained with H&E and observed with an optical microscope or underwent TUNEL staining and observation with a fluorescence microscope.

TUNEL analysis was performed with an In Situ Cell Death Detection kit (Sigma, St. Louis, MO, USA) according to the manufacturer's instructions. Briefly, sections of paraffin-embedded tissue with a thickness of 4  $\mu$ m were prepared. After dewaxing the paraffin by treatment with xylene and ethanol, proteinase K (20  $\mu$ g/mL in 10 mM Tris-HCl, pH 7.4) was added to the TUNEL reaction mixture. After washing with PBS, histology mounting medium (Fluoroshield with DAPI; Sigma Aldrich, St. Louis, MO, USA) was added, after which it was covered with a glass cover and observed with a fluorescence microscope (EVOS Digital Color Fluorescence Microscope; Invitrogen, Foster City, CA, USA).

#### 8-OHdG Assay

The amount of 8-OHdG in the tissue was measured with an 8-OHdG ELISA kit (Arigobio, Hsinchu, Taiwan) according to the manufacturer's instructions. Briefly, after adding a 10-fold homogenization buffer (0.1 M PBS, pH 7.4) to the cancer tissues, they were homogenized with a polytron homogenizer (Thomas Scientific, Gloucester County, NJ, USA) and centrifuged to use the supernatant as samples. DNA was extracted by using a G-spin Total DNA Extraction kit (iNtRON, Seongnam, Korea) with 200  $\mu$ L of the supernatant, which was treated with nuclease P1 (NEB, Ipswich, MA, USA) and used as DNA samples for 8-OHdG quantification. DNA samples (50  $\mu$ L) were placed in a 96-well plate, and each cell was treated with an HRP-conjugated 8-OHdG antibody. After reacting with the TMB substrate, absorbance was measured at 450 nm to quantify 8-OHdG.

#### TBARS Assay

A 10-fold homogenization buffer (0.1 M PBS, pH 7.4) was added to the cancer tissue, after which it was homogenized with a polytron homogenizer and used as a TBARS measurement sample. The contents of TBARS in tumor tissues were measured with the OxiSelect TBARS Assay Kit (Cell Biolabs, San Diego, CA, USA) according to the manufacturer's instructions.

#### Statistical Analysis

All measurement results were expressed as mean  $\pm$  SD. Experimental results were analyzed by analysis of variance (ANOVA) using the Statistical Package for the Social Sciences (SPSS, Ver. 12.0. SPSS Inc., Chicago, IL, USA), and the significance of differences between samples was defined as a P value of less than 0.05 on the Duncan multiple range test.

## Results

#### In Vitro PDT

The photocytotoxic effects of Photolon and iron in CT 26 cells were evaluated at 24 h after PDT at a light dose of 3 J/cm<sup>2</sup>. As shown in **Figure 1A**, photocytotoxicity increased in a Photolon dose-dependent manner at a light dose of 3 J/cm<sup>2</sup>. Photolon was phototoxic at concentrations above 6  $\mu$ g/mL. In addition, at iron concentrations of 8 mg/mL or higher, phototoxicity in cultured CT26 cells was higher for combined administration of Photolon and iron than for Photolon alone. To determine the effect of PDT on cellular lipid peroxidation, the lipid peroxide content of cells was measured by the MTT method (**Fig. 1B**). Cellular lipid peroxide content was higher after PDT, and PDT-induced lipid peroxide content was increased

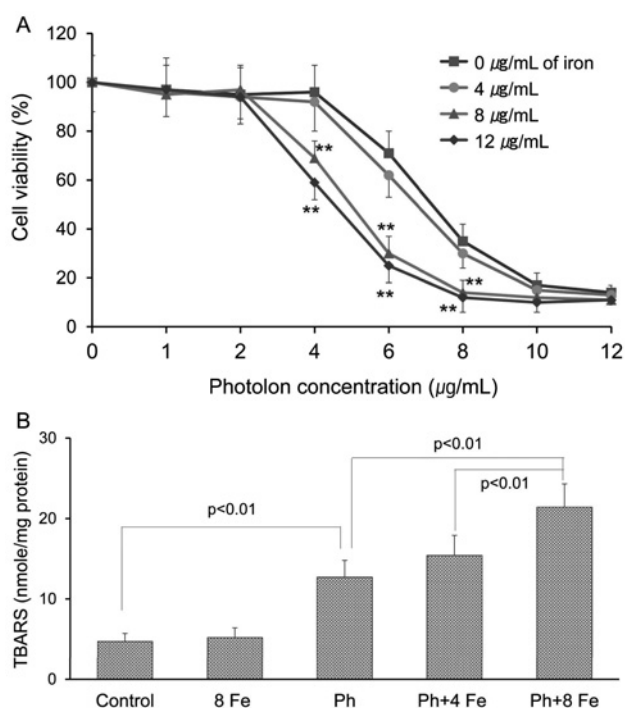


Fig. 1 Effect of iron on photocytotoxicity of Photolon in CT26 cells.

A: Viability of CT26 cells after PDT with Photolon and iron measured by an MTT assay.

B: Lipid peroxide content in CT26 cells after PDT with Photolon and iron.

by the addition of iron (8 µg/mL).

### Changes in Tumors After PDT in CT26 Tumor-Bearing Mice

To investigate the effect of PDT, we visually observed tumors up to 14 days after PDT in CT26 tumor-bearing mice (Fig. 2). Tumors grew continuously for up to 14 days in both the control and iron groups. In the PDT group, the skin of the laser irradiation site turned black on day 1. A crust that had formed on day 3 had shrunk on day 14 after PDT. In the iron+PDT group, the laser irradiation site turned black on day 1. A crust that had formed at the tumor site on day 3 was smaller on day 7, and part of the crust had fallen off on day 14. After that, crust shrinkage progressed further.

Tumor volumes measured up to 14 days after PDT are shown in Figure 3. The tumor volumes of the control group were  $229 \pm 65 \text{ mm}^3$  on day 0 and  $1,496 \pm 197 \text{ mm}^3$  on day 14—a 553% increase in tumor volume. The tumor volume of the iron group had increased by 590% on day 14, and there was no difference in tumor volume as compared with the control group. The tumor volumes in the PDT group were  $212 \pm 63 \text{ mm}^3$  and  $317 \pm 190 \text{ mm}^3$  on day 0 and day 14 after PDT, respectively. The tumor volume had increased by 49%. Therefore, the increase in tu-

mor volume was less than that in the control group ( $P < 0.01$ ). The tumor volumes in the iron+PDT group were  $209 \pm 58 \text{ mm}^3$  and  $57 \pm 101 \text{ mm}^3$  on day 0 and day 14 after PDT, respectively. Tumor volume on day 14 was 72% lower than the value on the day of PDT, and tumor volume on day 14 was smaller in the iron+PDT group than in the PDT group ( $P < 0.01$ ).

### Changes in Tumor Tissues After PDT in CT26 Tumor-Bearing Mice

Figure 4 shows H&E staining of tumor tissues at 24 h after PDT in CT26 tumor-bearing mice. H&E staining of tumor tissues in the control group and iron group revealed various sizes and shapes of nuclei in cancer cells; however, neither cell type nor nuclei differed between the 2 groups. The tumor tissues of the PDT group exhibited irregular nuclei and cells with unclear nuclear membranes. Furthermore, unclear nuclear membranes in the cells of tumor tissues were more common in the iron+PDT group than in the PDT group.

Figure 5A and 5B show the results of TUNEL staining of tumor tissues at 24 h after PDT in CT26 tumor-bearing mice. Many DAPI-stained cell nuclei were observed; however, few TUNEL-stained nuclei were observed in tumor tissues of the control and iron groups. In contrast, many TUNEL-stained cell nuclei were observed in the tumor tissue of the PDT group; the ratio of the number of TUNEL-stained nuclei to DAPI-stained nuclei was 45%. The number of TUNEL-stained nuclei was higher in the iron+PDT group than in the PDT group. The ratio of the number of TUNEL-stained nuclei to DAPI-stained nuclei was 69%-24% higher than that of the PDT group ( $P < 0.01$ ).

### Changes in 8-OHdG in Tumor Tissue After PDT in Tumor-Bearing Mice

Figure 6 shows the amount of 8-OHdG in tumor tissues at 24 h after PDT in CT26 tumor-bearing mice. There was no difference between the control and iron groups in the 8-OHdG content in tumor tissues. The 8-OHdG content of the tumor tissues in the PDT group was  $201.9 \pm 18.1 \text{ µg/g}$  tissue, which was 915% of the value for the control group ( $P < 0.01$ ), indicating that oxidative damage to the DNA of tumor cells was increased by PDT. The 8-OHdG content of tumor tissues was 33% greater in the iron+PDT group than in the PDT group ( $P < 0.01$ ); therefore, the increase in oxidative damage to the DNA of cancer cells was greater than that in the PDT group.

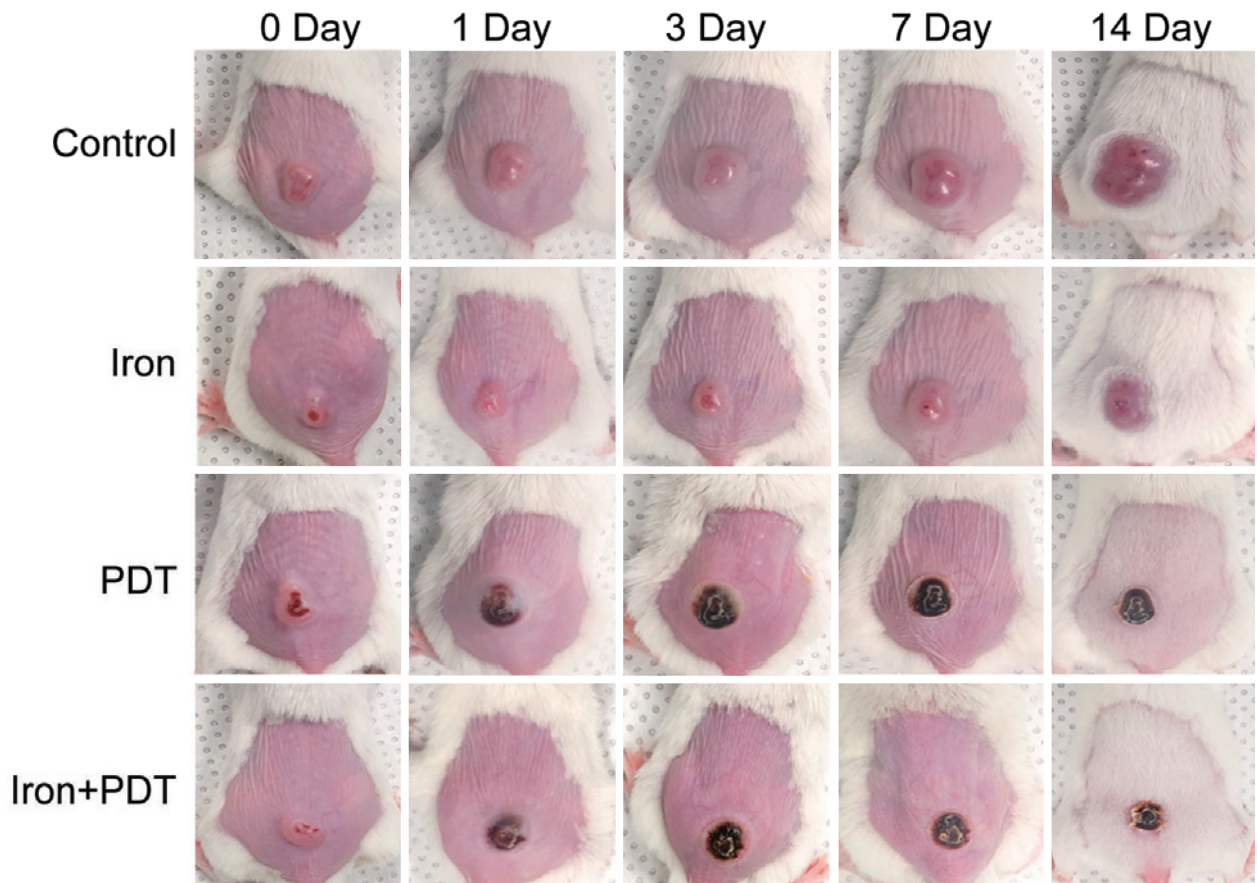


Fig. 2 Photograph of CT26 cancer-bearing mice after photodynamic therapy with Photolon (5 mg/kg) and laser irradiation (660 nm, 80 J/cm<sup>2</sup>).

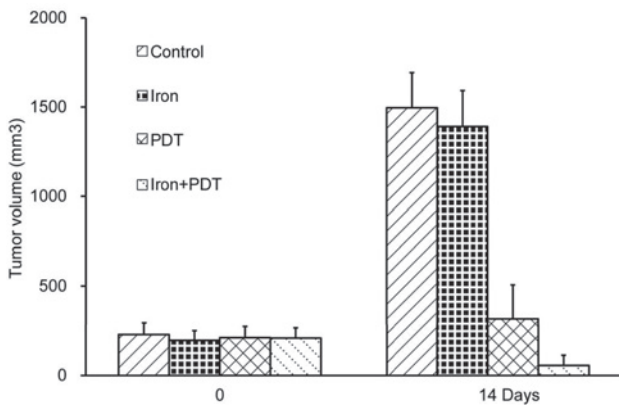


Fig. 3 Effects of iron (5 mg/kg BW) and PDT on tumor volume in CT26 cancer-bearing mice. Values are mean±SD, n=5. \*\*P<0.01.

### Changes in TBARS in Tumor Tissues After PDT in Tumor-Bearing Mice

Figure 7 shows TBARS content in tumor tissue at 24 h after PDT in CT26 tumor-bearing mice. There was no difference between the control and iron groups in TBARS content in tumor tissues. The TBARS content in the PDT group was 291 ± 41 μM/g tissue, 219% that of the con-

trol group (P<0.01), indicating that the lipid peroxide content in tumor tissues was increased by PDT. The TBARS content in the tumor tissues of the iron+PDT group was 46% higher than that of the PDT group (P<0.01), indicating greater lipid peroxidation when PDT was performed after iron administration as compared with PDT alone.

### Discussion

Iron has been shown to increase the anti-cancer effects of PDT. To determine the effect of iron on the effectiveness of PDT, this study assessed the effects of PDT after iron administration in CT26 cancer-bearing mice. CT26 cells are a murine colon carcinoma cell line derived from colon cancer tissues of BALB/c mice, and CT26-bearing mice are used for cancer treatment experiments involving PDT<sup>17</sup>. In cultured CT26 cells, Photolon phototoxicity was increased by PDT in a dose-dependent manner; at an iron concentration of 8 mg/mL or higher, the photocytotoxicity of Photolon and iron was higher than that of Photolon alone.

In CT26 cancer-bearing mice, the skin color at the tu-

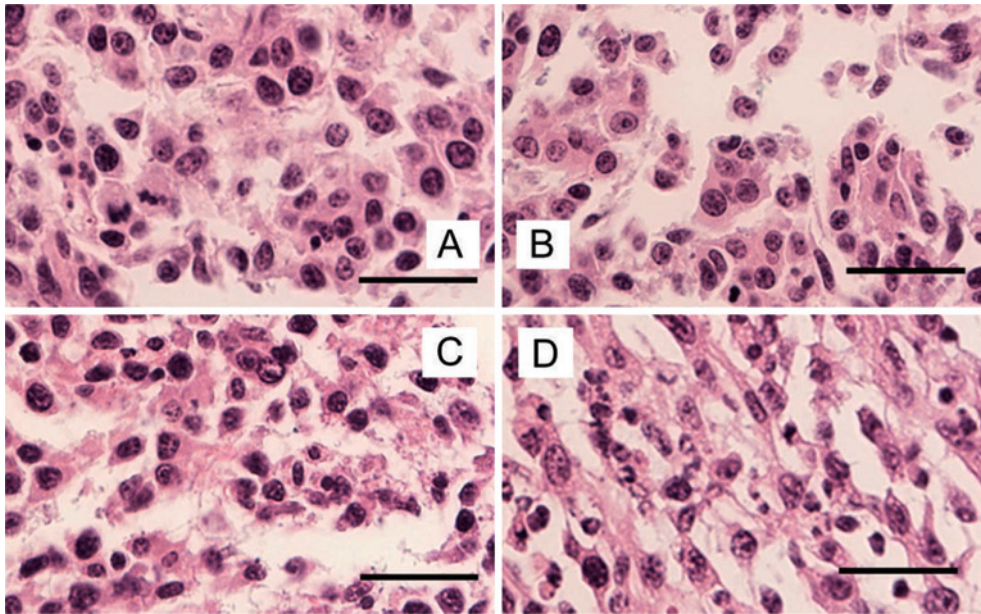


Fig. 4 H&E staining of tumor tissue at 24 h after PDT in CT26 cancer-bearing mice. A: control group, B: iron group, C: PDT group, D: Iron+PDT group  $\times 400$  magnification; scale bars=400  $\mu\text{m}$ .

mor site turned black on day 1 after PDT, a crust formed on the skin on day 3, and the crust had shrunk on day 14. A crust forms when exudate caused by skin damage dries on the skin. The crust that formed at the laser irradiation site after PDT was likely caused by damage to skin tissue and subcutaneous cancer tissues.

In cells, an irregular nuclear shape is associated with decreased cellular energy levels, and damage to the nuclear membrane is associated with cell death<sup>18,19</sup>. In this experiment, H&E staining of cancer tissue in the PDT group revealed cells with an irregular nuclear shape and partially invisible nuclear membrane, which may be a result of damage to the nuclear membrane.

In the iron+PDT group, shrinkage and peeling of the crust progressed faster than in the PDT group, and there were more cells without a nuclear membrane than in the PDT group in H&E staining of cancer tissues, suggesting that cancer cell damage was greater.

Tumor volumes were higher in the control and iron groups that did not receive PDT; however, there was no difference in the rate of increase in tumor volume between these groups. In the PDT group, the tumor volume growth rate was lower than in the control group, and the volume was smaller than in the control group on day 14, suggesting that carcinoma growth was suppressed by PDT. The tumor volume of the iron+PDT group was even lower, indicating that the anti-cancer effect was greater when PDT was performed after iron administra-

tion.

The photosensitizer used in this experiment, Photolon, is made by conjugating chlorine e6 and polyvinylpyrrolidone (Fig. 8) and is widely used in PDT studies<sup>20,21</sup>. Photolon accumulates in lysosomes, mitochondria, and ROS; photodamage of mitochondria and lysosomes by Photolon accumulation is important in PDT-mediated apoptosis<sup>22</sup>. Activation by light at a wavelength of 660 nm generates ROS, which cause oxidative damage to cancer cells, thereby exerting anti-cancer effects<sup>20</sup>.

Increased ROS in cells can induce chromosomal DNA fragmentation, and an increase in chromosomal DNA fragmentation can cause cell death from apoptosis or necrosis<sup>21</sup>. A study using a human biliary cancer cell line found that the number of TUNEL-positive cells was higher at 24 h after PDT<sup>23</sup>. In the present study, the proportion of TUNEL-positive cells in tumor tissues in the PDT group was 45% at 24 h after PDT, suggesting that DNA damage was caused by PDT. Furthermore, the proportion of TUNEL-positive cells was 22% higher in the iron+PDT group than in the PDT group. Therefore, iron might further increase DNA damage in cancer cells during PDT. The greater number of TUNEL-positive cells in the iron+PDT group than in the PDT group was a result of increased chromosomal DNA fragmentation in the cancer cells of the iron+PDT group. Therefore, the anti-cancer effect of PDT and iron administration may be the result of increased chromosomal DNA fragmentation.

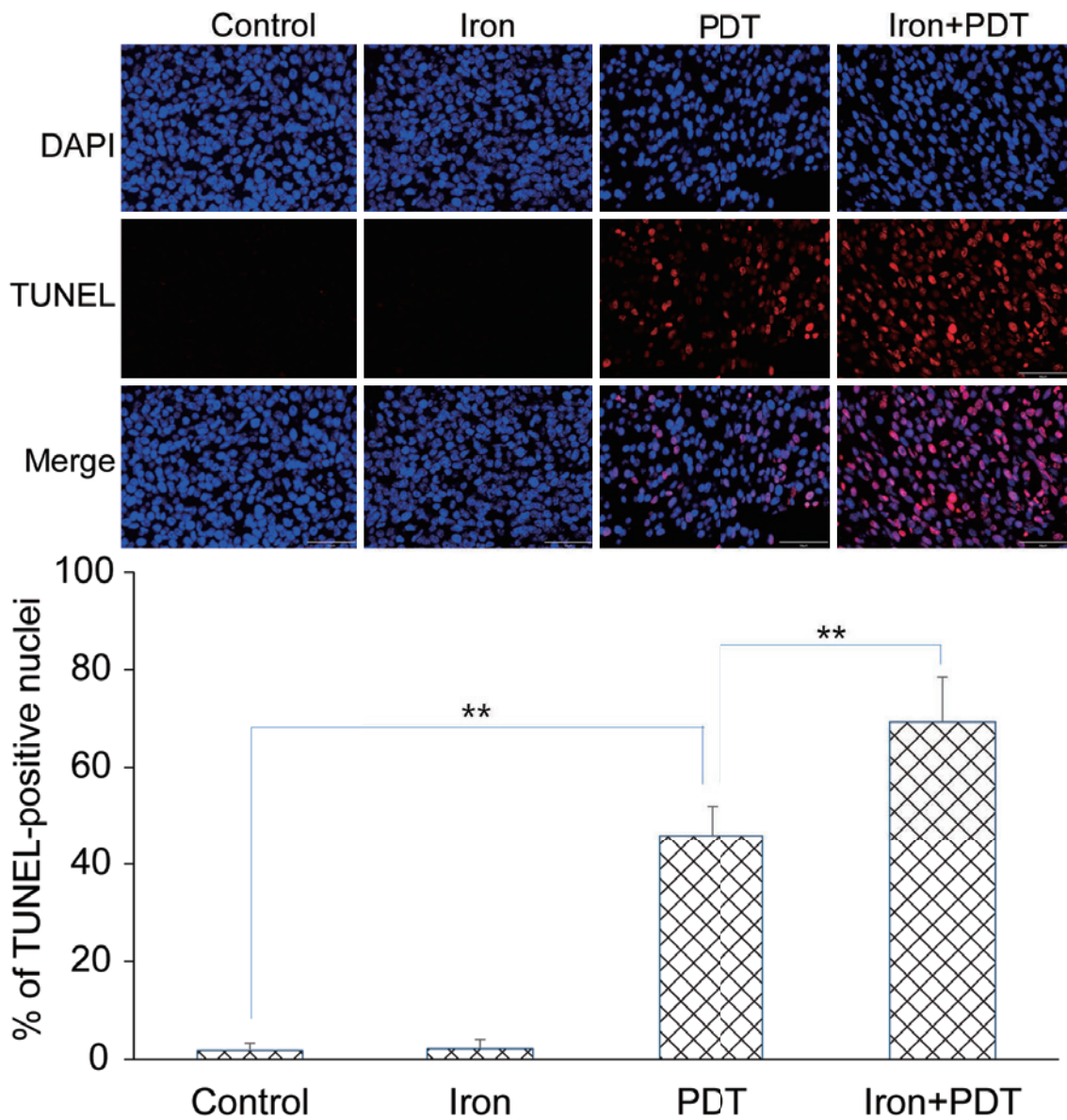


Fig. 5

A: TUNEL images of cancer tissue of CT26 cancer-bearing mice at 24 h after PDT.

DAPI: 6-diamidino-2-phenylindole  
 ×400 magnification; scale bars=400 μm

B: Effects of iron and PDT on TUNEL-positive nuclei content in tumor tissue of CT26 cancer-bearing mice. TUNEL-positive nuclei are defined as the percentage of all counted nuclei in random fields. Values are mean±SD, n=3. \*\*P<0.01.

ROS can produce 8-OHdG by acting on DNA; therefore, 8-OHdG has been used as a marker of cellular oxidative damage<sup>24</sup>. In this experiment, the 8-OHdG content in the tumor tissue of the PDT group was 915% that of the control group, suggesting that oxidative damage to the DNA of tumor cells was higher for PDT. The 8-OHdG content in tumor tissues was 33% higher in the iron+PDT group than in the PDT group, indicating that oxidative DNA damage was greater than that in the PDT group. Idarubicin (4-demethoxydaunorubicin), an anthra-

cycline anti-cancer agent that generates ROS, increases production of 8-OHdG when co-administered with copper, thereby increasing DNA damage<sup>25</sup>. In this experiment, 8-OHdG content in tumor tissues was 33% higher in the iron+PDT group than in the PDT group, suggesting that PDT-induced DNA oxidative damage in cancer cells was further increased by iron administration.

Lipid peroxidation caused by oxidative stress can induce apoptosis due to cell membrane dysfunction. TBARS is used as a marker of lipid peroxidation<sup>26,27</sup>. In

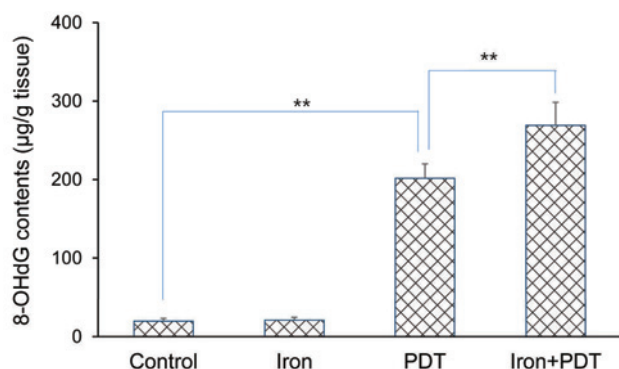


Fig. 6 Effects of iron and PDT on 8-hydroxy-2'-deoxyguanosine (8-OHdG) content in the tumor tissue of CT26 cancer-bearing mice. Values are mean±SD, n=3. \*\*P<0.01.

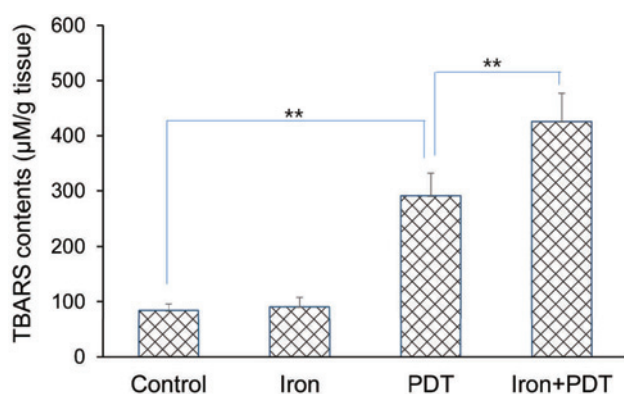


Fig. 7 Effects of iron and PDT on thiobarbituric acid reactive substance (TBARS) content in tumor tissue of CT26 cancer-bearing mice. Values are mean±SD, n=3. \*\*P<0.01

this study, lipid peroxide content in cultured CT26 cells was higher in the PDT group, which suggests that oxidative cell damage was increased by PDT. In addition, lipid peroxide content in cultured CT26 cells after PDT was increased by the addition of iron, suggesting that iron increases oxidative cell damage by PDT.

TBARS content in tumor tissues was higher in the PDT group than in the control group, suggesting that oxidative lipid damage in tumor tissues was increased by PDT. TBARS content in tumor tissues of the iron+PDT group was 46% higher than that in the PDT group, suggesting that oxidative damage to lipids was increased by PDT after iron administration.

Iron increases production of highly reactive hydroxyl radicals via the Fenton reaction. Therefore, it is thought that ROS were produced by PDT and that the number of hydroxyl radicals increased in the presence of iron, which caused lipid peroxidation. When iron supplements are injected into rats, the iron concentration in tissue cells

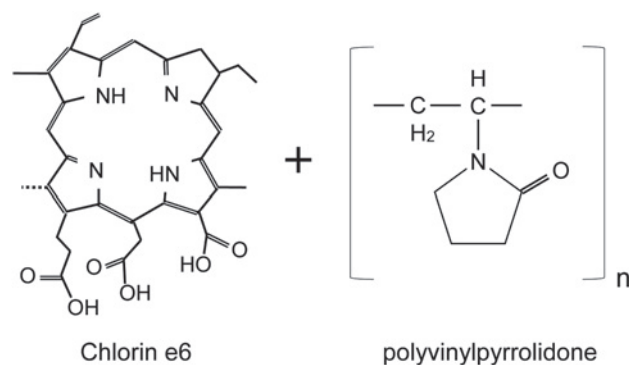


Fig. 8 Chemical structure of the photosensitizer Photolon

increases and this increased iron in cells induces ferroptosis. A Ce6-erastin nanodrug made from the ferroptosis inducer erastin and photosensitizer chlorin e6 increases the anti-cancer effects of PDT<sup>11</sup>. Ferroptosis is associated with an increase in lipid peroxide levels. In the present study, the increase in the amount of TBARS in the tumor tissue in the iron+PDT group was likely related to increased ferroptosis in the iron+PDT group. Our results show that intraperitoneal injection of an iron supplement (Venoferrum) increases the anti-cancer effect of PDT using Photolon, presumably because of the effects of ferroptosis.

#### Study Limitations

A limitation of this study is that the number of animals used in the experiment was insufficient, as we used a small number of animals in each experimental group. Therefore, additional research is necessary.

#### Conclusions

In a CT26 tumor-bearing mouse model, iron administration increased the anti-cancer effect of PDT using Photolon. This increase in the anti-cancer effects of PDT after iron administration is likely related to increased oxidative cell damage by ferroptosis.

**Conflict of Interest:** None declared.

#### References

1. Siegel RL, Miller KD, Jemal A. Cancer statistics, 2020. *CA Cancer J Clin.* 2020;70(1):7–30. doi: 10.3322/caac.21590
2. Martínez-Campa C, Alonso-González C. Editorial for the special issue "New strategies in cancer pharmacotherapy: Development of hormonal antineoplastic drugs, cytotoxic drugs and targeted therapies". *Int J Mol Sci.* 2020 8;21(11):4081. doi: 10.3390/ijms21114081
3. Kim J, Jo YU, Na K. Photodynamic therapy with smart nanomedicine. *Arch Pharm Res.* 2020;43(1):22–31. doi: 10.1007/s12272-020-01214-5
4. Zhang Q, Li L. Photodynamic combinational therapy in cancer treatment. *J BUON [Internet].* 2018 [cited 2020 Jun

- 18];23(3):561–7. Available from: <https://www.jbuon.com/archive/23-3-561.pdf>
5. Dolmans DE, Fukumura D, Jain RK. Photodynamic therapy for cancer. *Nat Rev Cancer*. 2003;3(5):380–7. doi: 10.1038/nrc1071
  6. Hayyan M, Hashim MA, AlNashef IM. Superoxide ion: Generation and chemical implications. *Chem Rev*. 2016; 116(5):3029–85. doi: 10.1021/acs.chemrev.5b00407
  7. Jaishankar M, Tseten T, Anbalagan N, Mathew BB, Beeregowda KN. Toxicity, mechanism and health effects of some heavy metals. *Interdiscip Toxicol*. 2014;7(2):60–72. doi: 10.2478/intox-2014-0009
  8. Mou Y, Wang J, Wu J, He D, Zhang C, Duan C, Li B. Ferroptosis, a new form of cell death: opportunities and challenges in cancer. *J Hematol Oncol*. 2019;12(1):34. doi: 10.1186/s13045-019-0720-y
  9. Shen Z, Song J, Yung BC, Zhou Z, Wu A, Chen X. Emerging strategies of cancer therapy based on ferroptosis. *Adv Mater*. 2018;30(12):e1704007. doi: 10.1002/adma.201704007
  10. Su Y, Zhao B, Zhou L, et al. Ferroptosis, a novel pharmacological mechanism of anti-cancer drugs. *Cancer Lett*. 2020;483:127–36. doi: 10.1016/j.canlet.2020.02.015
  11. Zhu T, Shi L, Yu C, et al. Ferroptosis promotes photodynamic therapy: Supramolecular photosensitizer-inducer nanodrug for enhanced cancer treatment. *Theranostics*. 2019;9(11):3293–307. doi: 10.7150/thno.32867
  12. Bridges R, Lutgen V, Lobner D, Baker DA. Thinking outside the cleft to understand synaptic activity: contribution of the cystine-glutamate antiporter (System xc-) to normal and pathological glutamatergic signaling. *Pharmacol Rev*. 2012;64(3):780–802. doi: 10.1124/pr.110.003889
  13. Qin J, Zhou C, Zhu M, et al. Iron chelation promotes 5-aminolaevulinic acid-based photodynamic therapy against oral tongue squamous cell carcinoma. *Photodiagnosis Photodyn Ther*. 2020;31:101907. doi: 10.1016/j.pdpdt.2020.101907
  14. Curnow A, Pye A. The importance of iron chelation and iron availability during PpIX-induced photodynamic therapy. *Photonics Lasers Med*. 2015;4(1):39–58. doi: 10.1515/plm-2014-0034
  15. Berg K, Anholt H, Bech O, Moan J. The influence of iron chelators on the accumulation of protoporphyrin IX in 5-aminolaevulinic acid-treated cells. *Br J Cancer*. 1996;74(5): 688–97. doi: 10.1038/bjc.1996.423
  16. Dogra Y, Ferguson DCJ, Dodd NJF, Smerdon GR, Curnow A, Winyard PG. The hydroxypyridinone iron chelator CP 94 increases methyl-aminolevulinic acid-based photodynamic cell killing by increasing the generation of reactive oxygen species. *Redox Biol*. 2016;9:90–9. doi: 10.1016/j.redox.2016.07.002
  17. Sanovic R, Verwanger T, Hartl A, Krammer B. Low dose hypericin-PDT induces complete tumor regression in BALB/c mice bearing CT26 colon carcinoma. *Photodiagnosis Photodyn Ther*. 2011;8(4):291–6.
  18. Tocco VJ, Li Y, Christopher KG, et al. The nucleus is irreversibly shaped by motion of cell boundaries in cancer and non-cancer cells. *J Cell Physiol*. 2018;233(2):1446–154. doi: 10.1002/jcp.26031
  19. Martelli AM, Zweyer M, Ochs RL, et al. Nuclear apoptotic changes: an overview. *J Cell Biochem*. 2001;82(4): 634–46. doi: 10.1002/jcb.1186
  20. Ding D, Zhong H, Liang R, et al. Multifunctional nanodrug mediates synergistic photodynamic therapy and MDSCs-targeting immunotherapy of colon cancer. *Adv Sci (Weinh)*. 2021;8(14):e2100712. doi: 10.1002/advs.202100712
  21. Chin WW, Lau WK, Heng PW, Bhuvaneshwari R, Olivo M. Fluorescence imaging and phototoxicity effects of new formulation of chlorin e6-polyvinylpyrrolidone. *J Photochem Photobiol B*. 2006;84(2):103–10. doi: 10.1016/j.photochem.2006.02.002
  22. Ali-Seyed M, Bhuvaneshwari R, Soo KC, Olivo M. Photolon™ --photosensitization induces apoptosis via ROS-mediated cross-talk between mitochondria and lysosomes. *Int J Oncol*. 2011;39(4):821–31.
  23. Higuchi Y. Chromosomal DNA fragmentation in apoptosis and necrosis induced by oxidative stress. *Biochem Pharmacol*. 2003;66(8):1527–35. doi: 10.1016/s0006-2952(03)00508-2
  24. Mai NNH, Yamaguchi Y, Chojjookhuu N, et al. Photodynamic therapy using a novel phosphorus tetraphenylporphyrin induces an anticancer effect via Bax/Bcl-xL-related mitochondrial apoptosis in biliary cancer cells. *Acta Histochem Cytochem*. 2020;53(4):61–72. doi: 10.1267/ahc.20-00002
  25. Graille M, Wild P, Sauvain JJ, et al. Urinary 8-OHdG as a biomarker for oxidative stress: A systematic literature review and meta-analysis. *Int J Mol Sci*. 2020;21(11):3743. doi: 10.3390/ijms21113743
  26. Gaschler MM, Stockwell BR. Lipid peroxidation in cell death. *Biochem Biophys Res Commun*. 2017;482(3):419–25. doi: 10.1016/j.bbrc.2016.10.086
  27. Moore K, Roberts LJ 2nd. Measurement of lipid peroxidation. *Free Radic Res*. 1998;28(6):659–71. doi: 10.3109/10715769809065821

(Received, March 4, 2022)

(Accepted, August 24, 2022)

Journal of Nippon Medical School has adopted the Creative Commons Attribution-NonCommercial-NoDerivatives 4.0 International License (<https://creativecommons.org/licenses/by-nc-nd/4.0/>) for this article. The Medical Association of Nippon Medical School remains the copyright holder of all articles. Anyone may download, reuse, copy, reprint, or distribute articles for non-profit purposes under this license, on condition that the authors of the articles are properly credited.